

Zinc Speciation in a Smelter-Contaminated Soil Profile Using Bulk and Microspectroscopic Techniques

DARRYL R. ROBERTS,*[†]
A. C. SCHEINOST,[‡] AND D. L. SPARKS[†]

Department of Plant and Soil Sciences, University of Delaware, Newark, Delaware 19717, and Department of Environmental Sciences, ETHZ, Switzerland

A soil profile contaminated as a result of Zn smelting operations from the historic Palmerton, PA smelting facility was characterized using X-ray absorption fine structure spectroscopy (XAFS) and X-ray diffraction (XRD) as bulk techniques, coupled with electron microprobe (EM), and microfocused XAFS as microscopic techniques to determine the chemical forms of Zn and elucidate its geochemical fate. The black, organic matter-rich topsoil contained 6200 mg/kg Zn and was strongly acidic (pH 3.2). Bulk XAFS revealed that about 2/3 of Zn was bound in franklinite and 1/3 bound in sphalerite. Both minerals may have been aerielly deposited from the smelter operation. Microspectroscopy detected also minor amounts of Zn adsorbed to Fe and Mn (hydr)oxides as inner-sphere sorption complexes, which may have formed after weathering of the Zn minerals. About 10% of the total Zn in this sample could be easily leached. In contrast, the yellowish, loamy subsoil contained less Zn (890 mg/kg) and had a higher pH of 3.9. XAFS revealed that Zn was mostly bound to Al-groups and to a lesser extent to Fe and Mn (hydr)oxides. Minor amounts of outer-sphere complexes or organic matter-bound Zn species could also be detected. About 70% of the total Zn content could be easily leached, indicating that outer-sphere sorption complexes have been underestimated and/or inner-sphere sorption complexes are weak due to the low pH. The Zn forms in the subsoil most likely derive from weathering of the Zn minerals in the topsoil. Due to the lack of minerals incorporating Zn and due to the low pH, the availability of Zn in the subsoil is as high as in the topsoil, while the total concentration is almost 1 order of magnitude smaller.

Introduction

The impact of smelting and processing of metal ores on environmental quality has been a major issue in industrialized countries for several decades. Often ore processing results in atmospheric emissions of acid and metals, resulting in

increased trace metal concentrations and acidic pH values in topsoils in the vicinity of smelter facilities. One significant metal contaminant in soils is zinc, which is mined in 50 countries and smelted in 21 countries (1). Zn ore processing releases also other elements associated with the ore body, thus introducing significant amounts of Cd and Pb to soils in addition to Zn. Under acidic, oxidizing conditions Zn is one of the most soluble and mobile of the trace metal cations (2) making it the most pytoxic microelement after Al and Mn (3). Consequently, soils near Zn smelters show a decline in the abundance of soil microorganisms, reduced soil fertility, damaged vegetation, and increased soil erosion (4). The environmental risk associated with Zn-impacted soils underscores the need to elucidate the fate of Zn introduced into soil environments.

Besides the solubility of primary metal-bearing phases such as ZnS (sphalerite), other processes may control the mobility and bioavailability of Zn, such as formation of secondary minerals, adsorption to soil minerals, or partitioning to soil organic matter (2). The fate of Zn is dependent on the environmental conditions such as pH, soil mineralogy, or organic matter content. Due to the inequilibrium in soils and the competition of potentially coexisting species for Zn there is often a continuum between the mechanisms for Zn²⁺ removal from solution. Since the degree of Zn mobility, and therefore bioavailability, is strongly dependent on its chemical forms, identification and quantification of potentially coexisting Zn forms is of paramount importance prior to making risk assessments and implementing remediation strategies.

Research investigating Zn sorption in simplified oxide and clay minerals systems and in soils displays its variable reactivity and speciation. Macroscopic sorption studies have shown that Zn can effectively adsorb onto Mn oxides (5–7), Fe (hydr)oxides, Al (hydr)oxides (8, 9), and aluminosilicates (10–12), with the extent of adsorption increasing with pH. At alkaline pH values, however, and at high initial Zn concentrations, the precipitation of Zn(OH)₂, Zn(CO)₃, and ZnFe₂O₄ may control Zn solubility (13, 14). Diffusion of Zn into the micropores of Fe oxides may effectively immobilize Zn in soils (15–17).

By employing X-ray absorption fine structure (XAFS) spectroscopy to investigate Zn sorption to oxides under neutral to basic pH values, researchers have demonstrated that Zn can form both inner-sphere surface complexes and Zn hydroxalcite-like phases upon sorption to Al-bearing minerals (18, 19); inner-sphere surface complexes on goethite (20); and both inner-sphere and multinuclear hydroxocomplexes on manganite (21). By applying XAFS and electron microscopy to Zn-contaminated soils and sediments, Zn has been demonstrated to occur as ZnS in reduced environments, often followed by repartitioning into Zn hydroxide and/or ZnFe hydroxide phases upon oxidation (22–24). Manceau et al. (25) used a variety of techniques, including XAFS and microfocused XAFS to demonstrate that upon weathering of Zn mineral phases Zn was removed from solution by the formation of Zn-containing phyllosilicates and, to a lesser extent, by adsorption to Fe and Mn (oxyhydr)oxides. These studies demonstrate that in any given system, Zn may be present in one of several forms making direct identification of each species with traditional approaches difficult.

While bulk XAFS has been successfully applied to characterize metal-contaminated environmental samples (22, 23, 27–30), one must realize that this technique probes a volume of several cubic millimeters, providing only one spectrum of the average species of the metal of interest. Deciphering the

* Corresponding author phone: (613)562-5800 ext. 6744; fax: (613)562-5190; e-mail: droberts@uottawa.ca. Mailing address: Department of Physics, 150 Louis Pasteur St., University of Ottawa, Ottawa, ON, Canada K1N 6N5.

[†] University of Delaware.

[‡] ETHZ.

single contributions to such an average spectrum is demanding requiring a complete database of reference spectra (31). Moreover, the signal from species coordinated to low Z elements only is often masked by the signal from species coordinated to high Z elements (25).

Microscopic techniques may resolve the different reactive sites in soil at the micron level, thus allowing for a more selective approach to speciation. Using electron microprobe analysis one can attain information on elemental correlations and contaminant distribution (24). However, the lower detection limit is often too high to study correlations between metals and possible sorbents, and the derivation of chemical forms from such correlations is difficult or even impossible (e.g., discrimination of Zn sulfate from Zn sulfide). Furthermore, electron diffraction of confined areas may identify crystalline minerals but must fail to detect noncrystalline species. Therefore, one of the most promising techniques to examine heterogeneous soil and environmental samples is microfocused XAFS (μ -XAFS), which is able to identify crystalline or noncrystalline species within a complex mixture on a micron scale (25, 32).

The objective of this study was to identify and semiquantify Zn species in a smelter-impacted soil by a variety of analytical techniques and to investigate the mobility of Zn in this soil using a stirred-flow desorption approach. Thereby, correlations between speciation and metal availability will be possible. The analytical techniques included XRD, electron microprobe, and synchrotron-based XAFS, μ -XAFS, and μ -X-ray fluorescence (XRF) spectroscopies. For the remainder of this paper, bulk XAFS will refer to both extended XAFS (EXAFS) and X-ray absorption near edge (XANES) spectroscopies. The term μ -XAFS will encompass both μ -EXAFS and μ -XANES.

Methods and Materials

Site Description and Sampling. Over 2000 acres of land on the north-facing slope of Blue Mountain have been contaminated from the emissions of the nearby Palmerton Zn smelting plant. The zinc smelting facilities (Smelters I and II) are located in east-central Pennsylvania near the confluence of Aquashicola Creek and the Lehigh River in the town of Palmerton (33). The first of two smelting plants was opened in 1898 by the New Jersey Zinc Company in order to process zinc sulfide (sphalerite) from ore brought in from New Jersey. In 1980 the plants stopped zinc smelting and in 1982 the U.S. EPA placed the area on its National Priorities List as a Superfund Site as a result of years of environmental degradation. The sphalerite ores contained approximately 55% zinc, 31% sulfur, 0.15% cadmium, 0.30% lead, and 0.40% copper (34). Over the 82 years the smelters produced approximately 47 Mg/year of Cd, 95 Mg/year of Pb, and 3575 Mg/year of Zn. Daily metal emissions since 1960 have ranged from 6000 to 9000 kg of Zn, from 70 to 90 kg of Cd, and less than 90 kg of Pb and Cu (34, 35). In addition to metals, sulfuric acid produced by the smelting processes has been deposited in surrounding areas, contributing to strongly acidic pH values of the soils. As a consequence of the phytotoxic effects of low pH and high metal concentrations, the dense forest vegetation of Blue Mountain was completely lost and soils on hill slopes almost completely eroded, exposing the underlying bedrock. Several attempts have been made to revegetate the site but thus far an effective remediation strategy has yet to be adopted (34).

Soil samples were collected along the Appalachian Trail, which follows the crest of the Blue Mountain SE of Palmerton. The most heavily contaminated soil collected from a profile directly above Smelter II was selected for more detailed experiments. The soil was collected from a pit between exposed bedrocks, where a shallow soil profile < 25 cm in depth persisted. The topsoil consisted of a 3–6 cm thick

layer of dark, hydrophobic organic debris consisting of only partially decomposed plant residues and soil organic matter. The accumulation of this amount of organic matter, which does not exist in surrounding forest soils, is an indication of drastically reduced biodegradation. The consolidated subsoil about 20 cm in thickness is most likely the remainder of the original Dekalb and Laidig series stony loams derived from shale, sandstone, and conglomerate (33). Undisturbed and bulk samples were collected from both topsoil and subsoil. The undisturbed samples, aggregates of several cm in diameter, were air-dried, embedded in acrylic resin (LR-White), cut, and polished into thin sections of various thickness (30–350 μ m). The bulk samples were air-dried and dry sieved to collect the <2 mm size fraction. Part of the latter fraction was dispersed in DDI water for 24 h, then sonified to break up aggregates, and wet sieved to collect the <250 μ m fraction. From the subsoil sample, dark concretions 0.5–2 mm in diameter were hand collected and ground in a mortar and pestle.

To create a library of Zn XAFS reference spectra, natural and synthetic Zn reference minerals and sorption samples were used. Franklinite (ZnFe_2O_4), hydrozincite ($\text{Zn}_5(\text{OH})_6(\text{CO}_3)_2$), and smithsonite (ZnCO_3) were provided by the Museum of Natural History, Washington, DC. Sphalerite (ZnS) was from Aldrich (99.9+% purity). Aqueous Zn^{2+} was prepared by dissolving 10 mmol/L $\text{Zn}(\text{NO}_3)_2$ (Zn nitrate, Aldrich, 99.9+% purity) in DDI H_2O and adjusting the pH to 6. A Zn–Al layered double hydroxide phase was synthesized in the laboratory following the method of Ford et al. (18). Sorption samples were prepared by reacting Zn with ferrihydrite (2-line, freshly precipitated) (36), high-surface area gibbsite (synthesized and aged 30 days, $90 \text{ m}^2 \text{ g}^{-1}$), birnessite ($45 \text{ m}^2 \text{ g}^{-1}$) (37), kaolinite (University of Missouri Source Clays Repository, Kga-1, cleaned, $10 \text{ m}^2 \text{ g}^{-1}$), hydroxy-Al interlayered vermiculite (Al-verm) (University of Missouri Source Clays Repository, Sanford vermiculite, cleaned, $90 \text{ m}^2 \text{ g}^{-1}$), and fulvic acid (Aldrich, 99% purity). All sorption samples were prepared in an N_2 atmosphere in a glovebox using ACS reagent grade chemicals and CO_2 -free DDI H_2O . To suspensions of 10 g/L solids and an ionic strength of 0.1 M NaNO_3 , Zn was slowly added from a 0.1 M $\text{Zn}(\text{NO}_3)_2$ stock solution to achieve Zn loadings of ca. $3.5 \mu\text{mol}/\text{m}^2$ for high-loading birnessite, $2.0 \mu\text{mol}/\text{m}^2$ for fulvic acid, $0.5 \mu\text{mol}/\text{m}^2$ for ferrihydrite, and $1.5 \mu\text{mol}/\text{m}^2$ for the remaining sorbents. The pH was adjusted to 6.0 ± 0.3 and maintained during a 24 h period. Solids were separated by centrifuging at 10 000 rpm for 10 min and stored in a refrigerator as wet pastes until analysis.

Analytical Methods. Soil pH was determined in 0.01 M CaCl_2 . Total metal concentration was measured using a $\text{HNO}_3/\text{HCl}/\text{HF}$ extraction followed by boric acid extraction (38). The solutions were analyzed using inductively coupled plasma mass spectrometry (ICP-MS) (39). Bulk mineralogy of the <250 μ m fraction of the soils was determined by powder X-ray diffraction using a Philips Norelco 1720 instrument equipped with a Cu tube (40 keV, 40 mA). Diffractograms were collected between 3° and $70^\circ 2\theta$ with 0.04° steps and a counting time of 5 s per step. Electron microprobe analysis was performed on resin-embedded thin sections (30–100 μ m thick) mounted on pure quartz slides, using a JEOL JXA-8600 microprobe equipped with wavelength dispersive spectrometers (WDS). Several elements (Si, Al, S, P, K, Ca, Zn, Mn, Fe, Pb) were mapped, and then the compositions of selected sample areas were determined with higher precision.

Bulk XAFS Spectroscopy. Zn K-edge (9659 eV) XAFS spectra of soil samples and Zn reference compounds were collected at beamline X-11A at the National Synchrotron Light Source (NSLS), Upton, NY. The electron storage ring operated at 2.5 GeV yielding an electron beam of 300–100 mA. The

double crystal Si(111) monochromator was detuned by reducing I_0 by 25%. The beam energy was calibrated by assigning the first inflection on the K-absorption edge of a Zn metal foil to an energy of 9659 eV. All samples were mounted into Teflon sample holders, sealed with Kapton tape, and run under ambient conditions (24 °C). The Zn reference minerals were diluted to 10 wt % in boron nitride to avoid self-absorption. Data were collected in fluorescence mode using a Stern-Heald-type (Lytle) detector filled with Kr gas and equipped with a Cu filter (40). To dampen the high background fluorescence from Fe in soil samples and the Zn-sorbed ferrihydrite, two to four sheets of Al foil were placed in front of the Cu filter. Depending on Zn and Fe concentrations, multiple scans were collected until satisfactory signal-to-noise ratios were achieved.

Micro-XAFS and μ -XRF. Thin sections of the topsoil sample were measured on beamline 10.3.2 of the Advanced Light Source (ALS), Lawrence Berkeley National Lab, Berkeley, CA. The higher brightness of GSECARS beamline 13-ID-C of the Advanced Photon Source (APS), Argonne National Lab, Chicago, IL enabled us to investigate the subsoil with lower metal concentration, and to measure μ -EXAFS instead of only μ -XANES. At both beamlines a pair of Si(111) channel-cut crystals were employed as monochromators, and the beam was focused down to approximately 2–5 μm using a set of grazing incidence, platinum-coated, elliptically bent, Kirkpatrick-Baez (K–B) focusing mirrors (41). Thin sections of the samples were placed on a digital x–y–z stage and set at an angle of 45° to the incident beam. Fluorescence X-rays were detected with either a Si solid-state detector (ALS) or a Ge 9-element detector (APS) positioned approximately 1–2 cm from the sample, depending on the Zn concentration in the sample. At the ALS, μ -XRF maps were collected over 800 \times 800 μm^2 areas with 5 μm step size and 500 ms dwell time. The beam energy was set to 11 keV during mapping. The μ -XANES spectra were collected on selected regions in the samples based on elemental associations obtained from μ -XRF mapping. μ -XANES spectra were collected from 100 eV below to 300 eV above the Zn K edge in step increments of 0.05 across the edge and 10 eV steps in the pre-edge region, with a dwell time of 10 s. The beam energy was calibrated with a Zn metal foil. At the APS, μ -XRF maps were collected over 300 \times 300 μm^2 areas with 5 μm step size and 500 ms dwell time. The μ -XAFS spectra were collected using the same settings as for the bulk-XAFS spectra collected at NSLS. To assess systematic deviations in XAFS data collection at the three different beamlines, selected reference samples were run at all beamlines. Independent of the beamline employed, μ -XAFS and bulk-XAFS spectra were highly reproducible.

XAFS Data Analysis. Both bulk and μ -EXAFS data extraction was performed using standard methods by extraction of k^3 -weighted chi spectra from the raw data and subsequent Fourier transformation over the range of 1.5–12 \AA^{-1} . Multishell fitting was done in R space over the range $\Delta R = 1.05$ –3.5 \AA with $\Delta k = 3.2$ –12 \AA^{-1} . Zn–O, Zn–S, Zn–Fe, Zn–Mn, Zn–Al, and Zn–Zn scattering paths were generated by FEFF7 (42) based on the structure of Zn-bearing minerals. The amplitude reduction factor, S_0^2 , was fixed at 0.85 during fitting. The errors in the bond distances (R) were estimated to be accurate to $R \pm 0.02$ \AA and $R \pm 0.05$ \AA , for the first and second shells, respectively, and coordination numbers (N) were accurate to $N \pm 20\%$ and $N \pm 40\%$ for the first and second shells, respectively. Error estimates were determined by a comparison of XRD and EXAFS results for franklinite and sphalerite, in agreement with estimates previously published (23, 43). In addition to the shell fitting approach, the soil samples were analyzed using direct least-squares fitting of the k^3 -weighted chi data using linear combination of known Zn references. This approach was used since conventional shell-by-shell fitting in multicomponent systems can lead to

impractically large values for the fitting parameters, and shells with a distance smaller than 0.1 \AA may not be separated at all (25, 28). During the fit the residuals were minimized which are defined as the normalized root square difference between the data and the fit (30). The accuracy of the fitting is dependent on the data quality, range of fitting, and how well the standards represent the unknown sample (30). Components with at least 10 wt % may be detectable by this method, and quantitative estimates are accurate to within plus or minus 25 wt % of the actual atomic fractions present (25, 28). A similar linear-combination approach was used to analyze the μ -XANES. The XANES fits were performed across the edge from 9640 to 9710 eV. All XAFS data analyses were performed with WinXAS 97 version 1.3 (44).

Desorption Experiments. The experimental setup for the Zn desorption studies from the contaminated surface and subsurface soils was similar to that illustrated by Strawn et al. (45). Briefly, a stirred-flow reaction chamber was connected to an HPLC pump at one end and to a fraction collector at the other end. A 0.2 M CaCl_2 solution adjusted to the pH of the soil was pumped through the chamber at a flow rate of 0.5 mL min^{-1} . The chamber was equipped with a 25 μm filter membrane with 0.2 μm pore size to separate the solid from the solution. The chamber volume of ca. 9 mL contained a suspension of 28 g L^{-1} soil, which was stirred at 400 rpm with a magnetic stir bar. Fractions of 5 mL were sampled at the chamber outlet and analyzed by atomic absorption spectrometry (AAS).

Results and Discussion

Soil Analysis. In the black topsoil, a Zn concentration of 6200 ± 480 mg/kg was present which decreased to 890 ± 80 mg/kg in the subsurface soil. The pH increased from 3.19 in the topsoil to 3.86 in the subsoil. With increasing distance from the Palmerton smelter furnace II, metal concentrations decreased (data not shown), suggesting that emissions from this furnace were the source of the contamination. Using XRD, quartz was found to be most abundant mineral in both topsoil and subsoil. In the subsoil, goethite, kaolinite, and gibbsite were detected. Diffractograms of the topsoil showed also peaks from franklinite (ZnFe_2O_4), a spinel-type mineral that often contains large amounts of Mn substituting for Fe and Mn (46). No Zn-bearing minerals were detected in the subsoil samples using XRD. Backscattered electron images (BSE) and selected elemental distributions collected by EM analysis are shown for the topsoil (top panel, Figure 1) and the subsoil (bottom panel, Figure 1). The main spherical entity in the topsoil image is an organic aggregate with moieties of metal bearing phases distributed throughout, indicated by the bright white spots in the BSE. The highest concentrations of Zn occur in spots measuring 1–4 μm in diameter, which are associated with Fe and S. Detailed quantitative WDS of such spots gave Fe/Zn ratios of 1:2 in agreement with those in franklinite and S/Zn ratios of about 1 indicating either Zn sulfide or sulfate. Regions of enriched Si and K are also present, most likely representing quartz and K-feldspars, respectively. In the subsoil, Zn and S concentrations were at or below the detection limit of the instrument, revealing little on potential phase distributions. Significant amounts of Al, Si, K, and Fe were detected, but no further quantitative analysis was performed to determine the exact mineralogy.

Bulk XAFS Analysis. The raw $\chi(k) \times k^3$ EXAFS data for the reference mineral and sorption samples are presented in Figure 2. Characteristic backscattering features of heavier elements assist in the initial identification of mineral samples, while sorbed samples show spectra dominated by backscattering from the first O shell, with the exception of the high-loading Zn birnessite sample. Fit results for these reference samples, using nonlinear, least-squares fitting of

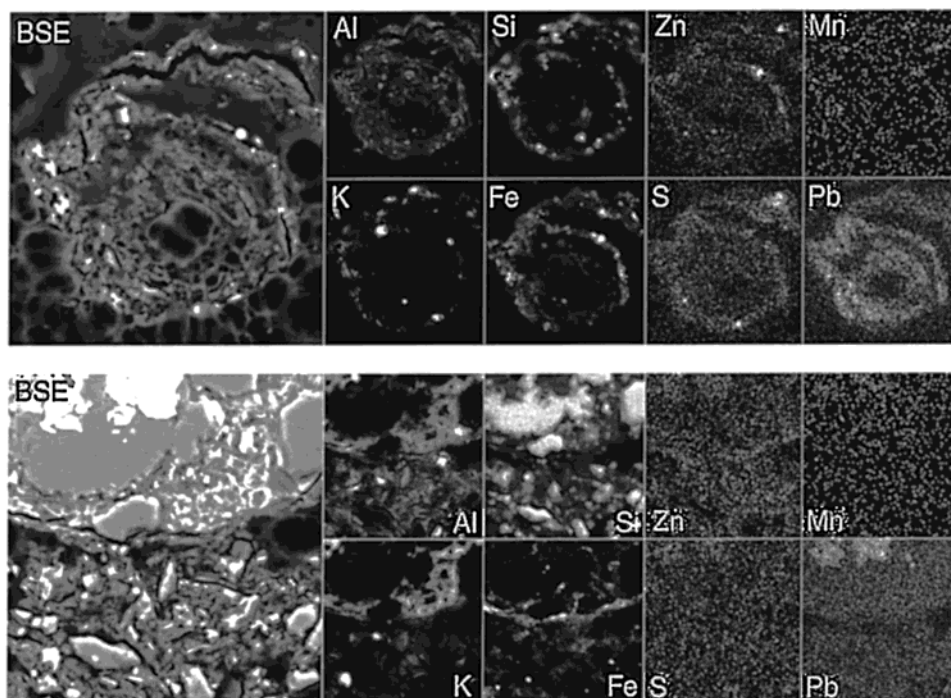


FIGURE 1. Representative backscattered electron (BSE) images and X-ray elemental dot maps for the surface soil (top panel) and the subsurface soil (bottom panel). White colors indicate a high concentration of target elements, black colors low concentrations.

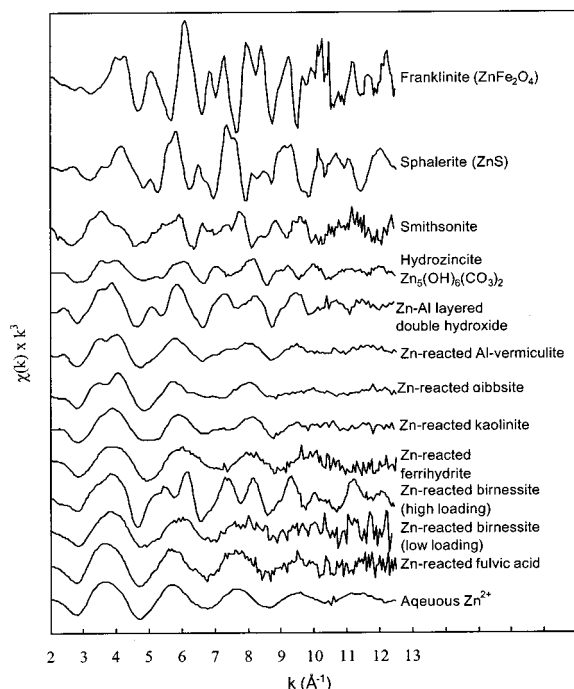


FIGURE 2. Normalized Zn-EXAFS k^3 -weighted χ spectra of reference samples used as empirical models for linear combination fitting.

individual coordination shells, are presented in Table 1. The weighted χ spectra and corresponding radial structure functions (RSFs) for the surface and subsurface samples are presented in the top panel of Figure 3. For the topsoil sample, Zn was found to be tetrahedrally coordinated to both O and S ($N \approx 4$, Table 2). The second shell contribution could be fit with a Zn distance of 3.49 Å. Coordination numbers and distances of the O shell and the Zn shell are in line with those of franklinite (compare with fit results for franklinite in Table 1). Coordination number and distance of the S shell are indicative of sphalerite (Table 1 and Table 2). The peaks in

the RSF from the range of 4.5–6 Å (Figure 3) are most likely a result of backscattering from another set of O or S and no attempts were made to fit these contributions. The linear combination fitting approach estimated 66% franklinite and 34% sphalerite for the topsoil sample (Table 3). Despite the large amount of organic material in this sample, adding the Zn-fulvic acid spectrum did not reduce the fit residual. Organic compounds generally yield a weak EXAFS signal, which can be masked by the more intense signal from inorganic compounds (25). Therefore, no definitive conclusion on the presence of Zn-organic complexes can be drawn from EXAFS. However, as a soft acid, Zn is not expected to significantly bind to organic matter, in contrast to transition acids such as Cu^{2+} and Ni^{2+} .

In the subsurface soil samples, the $\chi(k) \times k^3$ spectra have fewer, weaker beats, relative to the surface soil indicating a lack of significant higher-shell backscattering (Figure 3, top right panels). The χ spectra for the coarse (<2 mm) and fine (<250 μm) fractions of the soil have similar structural features, with a splitting of the first major oscillation at approximately 3.8 \AA^{-1} being the major distinction to the χ spectrum of the nodule sample (bottom spectrum). This feature has been attributed to the presence of 'light' Al atoms in the coordination shell of Zn by Manceau et al. (17). In agreement, our reference χ spectra of Zn sorbed to Al minerals show the same oscillation. Correspondingly, the second shell for the fine and coarse subsurface sample could be fit with approximately 1–2 Al atoms at distances of 3.04 and 3.06 Å, respectively (Table 2), indicating that Zn sorbs as inner-sphere sorption complex to Al–O, OH surface groups (compare to Zn–Al distances in Table 1). Coordination numbers and distances of the O shell of these samples are less conclusive. According to crystallographic data, the distance between O and Zn should be approximately 1.96 to 1.98 Å for tetrahedral coordination but 2.06 to 2.08 Å for octahedral coordination (19). While the coordination numbers for Zn-reacted Al minerals and the two size-fractions of the subsoil samples indicate octahedral coordination, the distances often show values between those expected for octahedral and tetrahedral coordination, suggesting their

TABLE 1. XAFS Parameters for Reference Mineral and Sorption Samples

sample	first shell				second shell			
	atom	CN ^{a,d}	R (Å) ^{b,e}	σ ² (Å ²) ^c	atom	CN ^f	R (Å) ^g	σ ² (Å ²)
franklinite, ZnFe ₂ O ₄	Zn-O	3.7	1.97	0.0030	Zn-Fe/Zn	11	3.50	0.0085
sphalerite, ZnS	Zn-S	3.9	2.34	0.0037	Zn-Zn	12	3.87	0.0079
smithsonite, ZnCO ₃	Zn-O	5.9	2.10	0.0028	Zn-Zn	7.8	3.71	0.0072
hydrozincite, Zn ₅ (OH) ₆ (CO ₃) ₂	Zn-O	4.1	2.02	0.0041	Zn-Zn	1.8	3.22	0.0061
Zn-Al LDH	Zn-O	5.9	2.07	0.0090	Zn-Al	2.4	3.06	0.0098
	Zn-Zn				Zn-Zn	4.3	3.08	0.0099
Zn-reacted Al-vermiculite	Zn-O	5.8	1.97	0.0090	Zn-Al	2.5	3.05	0.0051
Zn-reacted gibbsite	Zn-O	5.1	2.01	0.0097	Zn-Al	4.4	3.02	0.0080
Zn-reacted kaolinite	Zn-O	6.1	2.01	0.0135	Zn-Al	1.4	3.05	0.0012
Zn-reacted ferrihydrite	Zn-O	3.9	1.94	0.0050	Zn-Fe	1.9	3.34	0.0170
Zn-reacted birnessite (high loading)	Zn-O	5.6	2.07	0.0070	Zn-Mn	7.7	3.49	0.0085
Zn-reacted birnessite (low loading)	Zn-O	6.2	2.02	0.0085	Zn-Mn	0.8	3.47	0.0079
Zn-reacted fulvic acid, aqueous	Zn-O	6.8	2.06	0.0100				
aqueous Zn ²⁺	Zn-O	5.8	2.06	0.0070				

^a Coordination number. ^b Interatomic distance. ^c Debye-Waller factor. ^d Fit quality limits for parameters: ±20%. ^e ± 0.02 Å. ^f ± 40%. ^g ± 0.05 Å.

TABLE 2. XAFS Parameters for Soil Samples

sample	first shell				second shell			
	atom	CN ^{a,d}	R (Å) ^{b,e}	σ ² (Å ²) ^c	atom	CN ^f	R (Å) ^g	σ ² (Å ²)
bulk XAFS								
surface (<2 mm)	Zn-O	3.7	1.98	0.0071	Zn-Fe/Zn	11.2	3.49	0.0089
	Zn-S	3.8	2.35	0.0080				
subsurface (<2 mm)	Zn-O	5.7	2.08	0.0051	Zn-Al	1.2	3.04	0.0030
subsurface (<250 μm)	Zn-O	6.2	2.03	0.0065	Zn-Al	1.9	3.06	0.005 ^j
subsurface (nodules)	Zn-O	6.3	2.01	0.0070	Zn-Fe/Mn	1.1	3.46	0.0100
micro XAFS								
surface - spot 1 ^h	Zn-O	4.0	1.97	0.0079	Zn-Fe/Zn	13.2	3.52	0.0091
surface - spot 2	Zn-O	4.1	1.98	0.0070	Zn-Fe/Zn	8.1	3.51	0.0100
subsurface - spot 1 ⁱ	Zn-O	5.6	2.04	0.0049	Zn-Al	1.5	3.01	0.005 ^j
subsurface - spot 2	Zn-O	5.1	2.00	0.005 ^j	Zn-Fe	1.9	3.25	0.005 ^j
subsurface - spot 3	Zn-O	3.4	1.98	0.005 ^j	Zn-Fe/Mn	1.4	3.45	0.005 ^j

^a Coordination number. ^b Interatomic distance. ^c Debye-Waller factor. ^d Fit quality limits for parameters: ±20%. ^e ± 0.02 Å. ^f ± 40%. ^g ± 0.05 Å. ^h Spot number refers to random locations in surface sample. ⁱ Spot number refers to subsurface maps in the bottom panel of Figure 4. ^j Indicates value fixed during fitting.

simultaneous presence. This is to be expected from the lack of crystal field stabilization energy, which allows Zn(II) to easily switch between both types of coordination (47). Therefore, there is strong evidence that Zn is bound to Al surface groups in the two subsoil size fractions. These results were confirmed by the linear combination fit, where Zn-sorbed gibbsite represented most of the EXAFS signal for the <250 μm fraction (60%, Table 3). However, for the <2 mm fraction most of the EXAFS signal could be explained by aqueous Zn²⁺, a 20% increase relative to the Zn²⁺ contribution for the <250 μm fraction. This indicates that Zn is probably bound via outer-sphere complexation in the soils and this complex was altered upon fractionation in water. To a much lesser extent, spectra of Zn sorbed to ferrihydrite contributed to the spectra of the <250 μm fraction.

The EXAFS spectra of the blackish, Mn- and Fe-rich nodules separated from the subsoil sample could be fit with about 1 Mn or Fe atoms at a distance of 3.46 Å, indicating that Zn is sorbed to a either a Mn or Fe (hydr)oxide, or both simultaneously. With the linear combination fits, Zn sorbed to ferrihydrite and Zn sorbed to birnessite (low loading) were present in near equal portions (30 and 34% respectively, Table 3). Aqueous Zn²⁺ contributed approximately 25% and Zn sorbed to gibbsite only 10% of the total. The comparison between both fitting approaches clearly shows that the shell fitting tends to reveal only the species with the strongest second shell backscattering, while the linear combination fit reveals several other species including the aqueous one. In

combination, the results suggest that Zn resides in three species, sorbed as outer-sphere complexes and sorbed as inner-sphere complexes by both Al and Fe/Mn (hydr) oxides.

Microspectroscopic Analysis. The μ-XRF maps collected on the surface (top panel) and subsurface (bottom panel) soils are presented in Figure 4. The relative concentrations of the elements are represented by the scale bar at the right of each panel. The surface soil indicates a strong correlation between Zn and Fe in concentrated spots throughout the sample, similar to the EM results. Moreover, the Zn appears in more discrete particles relative to the subsurface soil. The three numbered arrows in the middle map (Zn) of the top panel represent spots where Zn μ-XANES spectra were collected (Figure 5). The spectrum of spot 3 was best fit by 100% franklinite; spot 2 by 80% sphalerite, 5% franklinite, and 15% Zn sorbed to ferrihydrite; and spot 1 by 88% franklinite, 7% Zn-ferrihydrite, and 5% Zn sorbed to birnessite (low loading), using the linear combination approach (Table 3, bottom). Micro-EXAFS data were collected on two randomly selected spots of the same thin section (Figure 3, bottom panels). Both shell fitting and linear combination fits showed the presence of franklinite, with the linear combination fit additionally showing the presence of Zn sorbed to ferrihydrite (Tables 2 and 3). Out of the five spots (3 μ-XANES, 2 μ-XAFS) taken on the surface soil, four out of five were dominated by franklinite and only one by sphalerite suggesting that franklinite is the most abundant phase in the

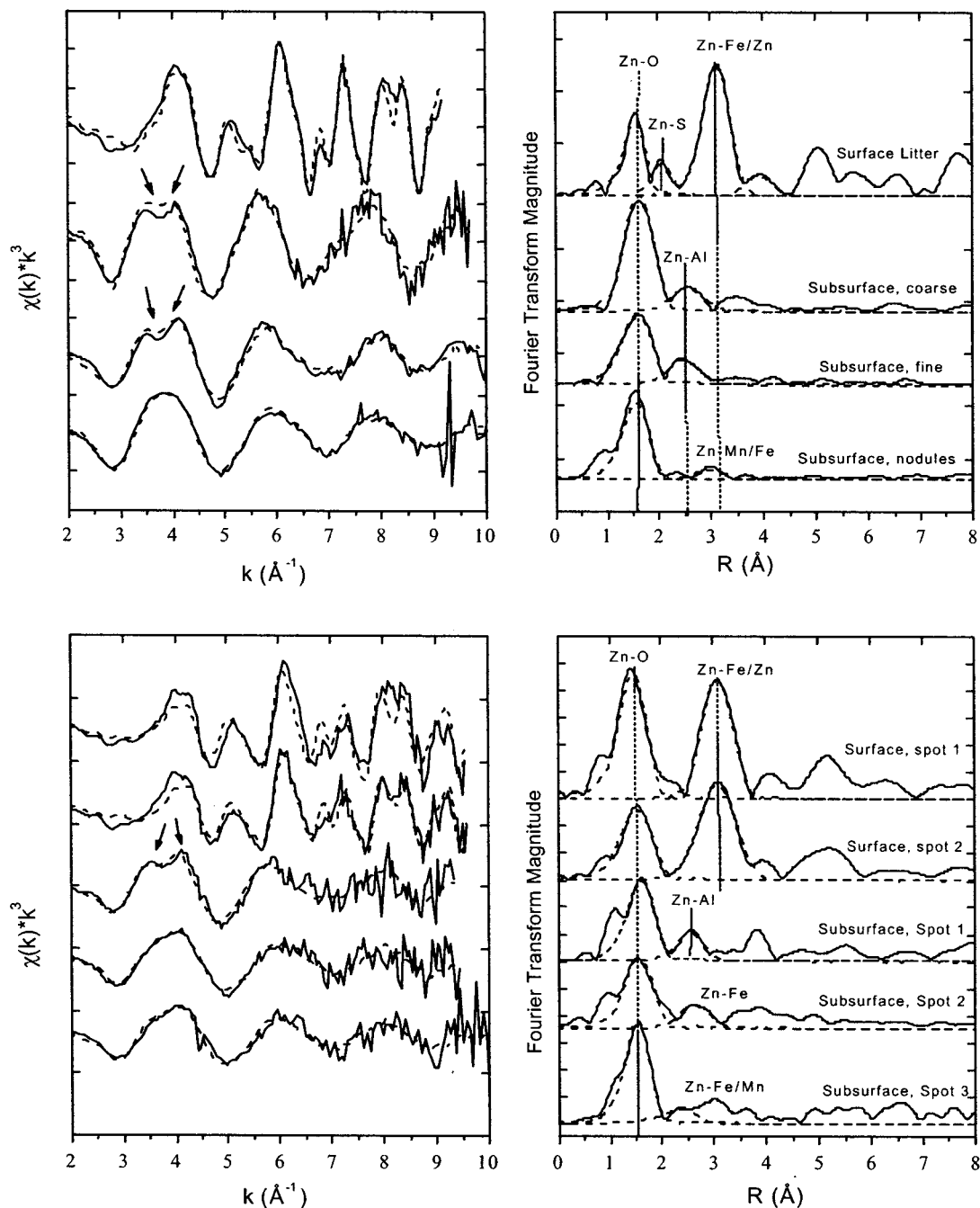


FIGURE 3. Normalized Zn-EXAFS k^3 -weighted chi (left panel) and corresponding Fourier transforms (right panel) of surface and subsurface samples using bulk (top panels) and μ -XAFS (bottom panels). In the left panels, the solid lines are the raw data and the dotted lines are fit results from linear combinations of chi data. In the right panels, solid lines represent experimental data and dashed lines represent results from nonlinear, least-squares fitting of individual shells.

sample, in agreement with results from bulk XAFS analysis and XRD.

The elemental maps of the subsoil sample show a strong spatial correlation between Zn and Mn and between Zn and Fe to a lesser extent (Figure 4, bottom panel). This suggests that Zn may be present in different phases over a small sample area. The chi spectrum (bottom left panel of Figure 3) of subsurface spot 1 shows the oscillation indicative of Al atoms at a distance of about 3.8 \AA^{-1} , similar to the bulk EXAFS results (top left panel of Figure 3). Correspondingly, both shell fit and linear combination fit provide evidence for the presence of an inner-sphere sorption complex between Zn and Al surface groups (Tables 2 and 3). The fit results from multishell fitting (Table 2) indicate that Zn is octahedrally

coordinated ($R_{\text{Zn-O}} = 2.04 \text{ \AA}$) and bound to an Al-bearing phase in this spot (approximately 1.5 Al atom @ 3.01 \AA), similar to the results from bulk XAFS on the fine and coarse fractions (Table 2). For spots 2 and 3, the Zn-O distance was more indicative of tetrahedral coordination ($R_{\text{Zn-O}} = 2.00$ and 1.98 \AA , respectively). Spot 2 had a $R_{\text{Zn-Fe}} = 3.25 \text{ \AA}$, while spot 3 could be fit with either an Fe or Mn atom at 3.45 \AA . Linear combination fit results indicate subsurface spot 1 was best fit with Zn-reacted gibbsite (50%) with contributions from aqueous Zn^{2+} (35%) and Zn-ferrihydrite (15%) (Table 3). Spots 2 and 3 were best fit with contributions from Zn-ferrihydrite, aqueous Zn^{2+} , Zn-birnessite (low loading), and Zn-gibbsite (Table 3). The most significant difference was in the Zn-birnessite contribution, which was not present in spot

TABLE 3. Linear Combinations of Fit Results for Soil Samples

	(%) ^a					
	ZnFe ₂ O ₄	ZnS	Zn-ferrhydrite	Zn-birnessite	Zn-gibbsite	Zn-aq
Bulk EXAFS						
surface	66	34	0	0	0	0
subsurface, <2 mm	0	0	10	0	30	60
subsurface, <250 μm	0	0	5	0	60	35
subsurface, nodules	0	0	30	34	10	26
Micro-EXAFS						
surface, spot 1	100	0	0	0	0	0
surface, spot 2	85	0	15	0	0	0
subsurface, spot 1	0	0	15	0	50	35
subsurface, spot 2	0	0	40	0	15	45
subsurface, spot 3	0	0	35	25	15	25
Micro-XANES						
surface, spot 1	88	0	7	5	0	0
surface, spot 2	5	80	15	0	0	0
surface, spot 3	100	0	0	0	0	0

^a Estimated error in fitting was ±25%.

2 but accounted for 25% of the Zn species in spot 3, agreeing with the observations from μ-XRF (Figure 4) and from shell fitting (Table 2) in which either Mn or Fe could be fit in the second shell of spot 3. These results aid in confirming the results from bulk XAFS and indicate mixed Zn speciation, even on a micron size scale.

Zinc Desorption Behavior. Figure 6 displays the results from the stirred-flow desorption experiments. After leaching

with 70 chamber volumes of 0.1 M Na(NO₃)₂ at soil pH, nearly 65% of total Zn was removed from the subsoil but only 11% from the topsoil sample. Moreover, the subsurface sample released Zn more rapidly, with over 60% of the total Zn removed from the soil after only five chamber volumes as compared to a more gradual release from the surface material. In terms of total amounts, 620 mg/kg Zn were released from the subsoil and 800 mg/kg from the topsoil. Thus, almost similar amounts were released from both horizons, although the topsoil Zn concentration was about an order of magnitude higher than the subsoil concentration. In the surface soil, we suspect that Zn is released from sphalerite rather than franklinite since sphalerite is unstable in oxidizing environments and franklinite is quite insoluble (48). In addition, some labile Zn may be associated with the organic matter in this sample that was not well detected using our approach. The gradual release of Zn from this sample with time suggests the Zn source is slowly dissolving (i.e., sphalerite). In the subsurface soil, the Zn is rapidly released initially followed by a slower desorption step. In this case, we postulate that labile Zn that is adsorbed as an outer-sphere complex or to organic matter is initially removed followed by a slower removal due to Zn bound to Al minerals/oxides and Fe oxides as inner-sphere complexes.

Environmental Significance. The presence of franklinite and sphalerite in the topsoil can be explained by the history of the smelting facility. The main Zn ore used in the smelting process at Palmerton was sphalerite. During smelting, sphalerite is exothermally converted at 900 °C to zinc oxide, a more soluble Zn mineral phase (49). Due to the presence of significant amounts of iron in the sphalerite ores, zinc ferrite (ZnFe₂O₄, franklinite) also forms during the roasting process, and given smelting inefficiencies, portions of this

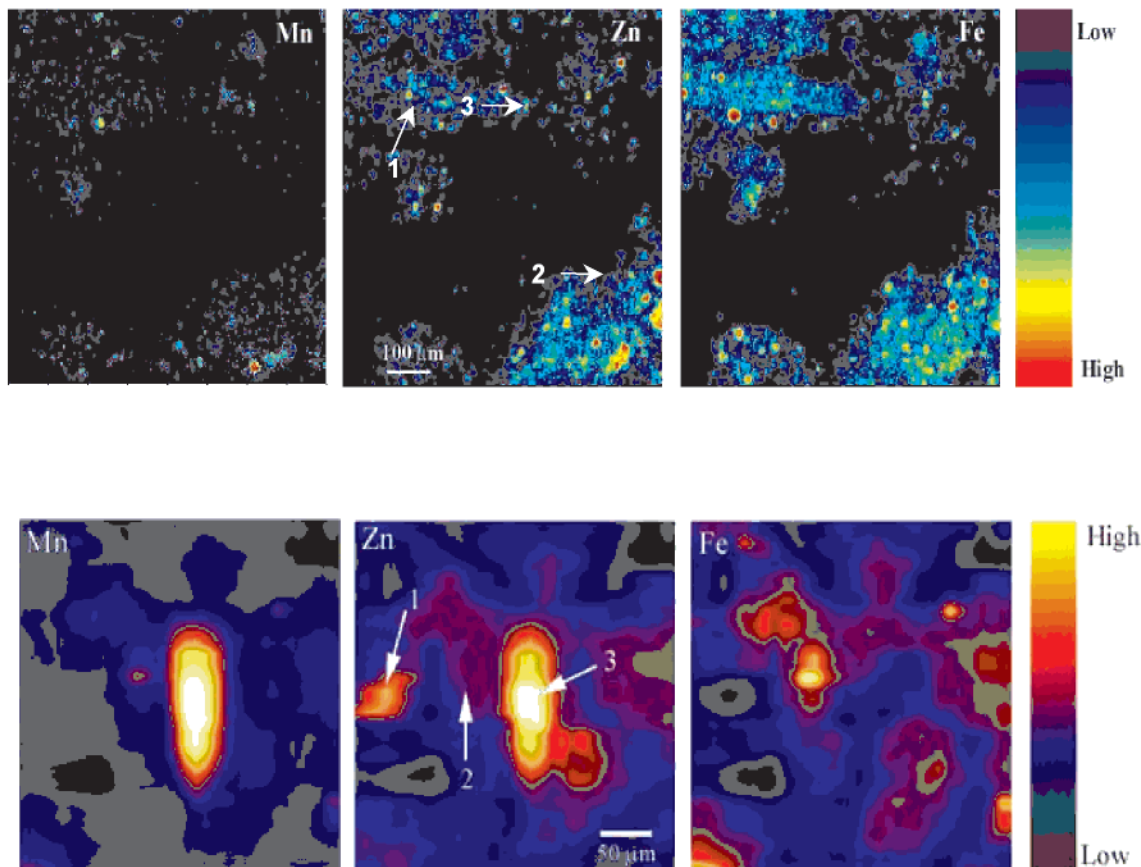


FIGURE 4. Micro-XRF maps for the surface (top panel) and subsurface (bottom panel) soil samples. The numbered arrows indicate spots where μ-XAFS spectra were collected. The color bars to the right are in arbitrary units with the darkest color corresponding to lowest concentration and brightest color corresponding to highest concentration.

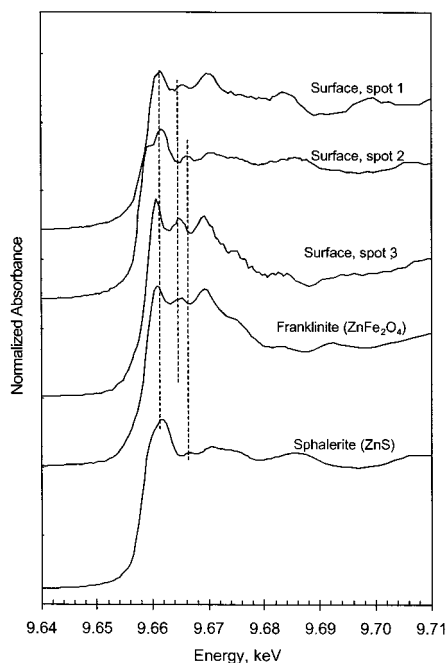


FIGURE 5. Micro-XANES spectra of surface sample from spots indicated in Figure 4 (top three spectra) and franklinite and sphalerite references (bottom two spectra). The lines serve as guides to help distinguish between phases.

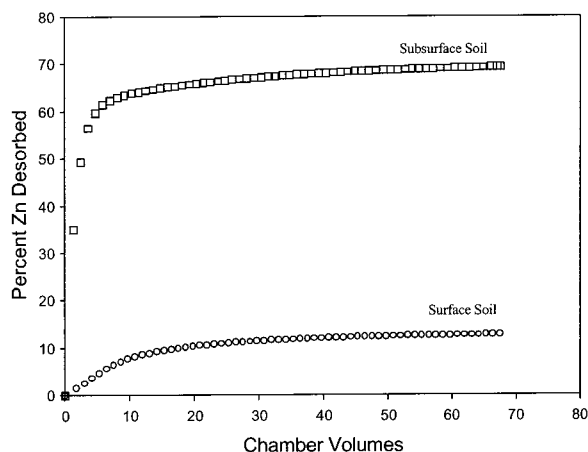


FIGURE 6. Zn desorption from surface and subsurface soil samples represented by amount of Zn released relative to total amount in sample.

material are released as atmospheric emissions along with nonsmelted sphalerite. Since the topsoil is exposed to the atmosphere, one would expect ZnS to oxidize and release Zn and SO_4^{2-} and therefore not be present anymore several decades after the smelting operation has been canceled. However, biological activity in this surface material is probably minimal due to deposition of sulfuric acid, and limited microbial oxidation of sphalerite may explain its persistence. Also, Pb and Cd present in the sphalerite may decrease its solubility. The stability of franklinite in the topsoil is in line with solubility estimates (13). A study by Venditti et al. (50) on soils contaminated as a result of metallurgical activities also revealed the persistence of sphalerite and franklinite in contaminated agricultural soils.

The presence of aqueous or outer-sphere Zn^{2+} and of Zn sorption complexes on Al and Mn/Fe (hydr)oxides in the subsoil implies that Zn^{2+} has been released from the Zn-bearing phases in the surface soil and transported to the underlying soil where it was partially readsorbed to both Al

and Fe/Mn oxides. Our results vary slightly from recent investigations by Manceau et al. (25) on Zn-contaminated smelter soils in which Zn was predominately bound in neoformed Zn-containing phyllosilicates and only to a lesser extent bound to Mn and Fe (hydr)oxides. The difference can be explained by the higher pH (5.5 or greater) and the higher Zn concentrations in subsoils in the study by Manceau et al. study (25), conditions which make the precipitation of phyllosilicates more favorable. Due to the more acidic pH of the Palmerton subsoil, Zn remains largely available, as was shown by the desorption experiment. Clearly, increasing the pH of the site will help immobilize Zn to a greater extent.

The results of our study show the importance of combining several spectroscopic techniques to accurately determine Zn speciation in soils as no one technique is capable of completely characterizing a system. Furthermore, our results clearly indicate that Zn speciation, rather than total Zn concentration is controlling Zn desorption from these soils. To our knowledge this is the first study that has directly identified Zn species in surface and subsurface soils in the Palmerton area, and the results should prove valuable in developing an effective remediation strategy.

Acknowledgments

The authors are grateful to the staff at beamlines X-11a at the National Synchrotron Light Source, 10.3.2 at the Advanced Light Source, and the 13-ID-C at the Advanced Photon Source for assistance in collecting XAFS data. We especially appreciate the assistance of Stephen Sutton and Matt Newville at the APS in assisting with our data collection. We thank Brian McCandless (Institute of Energy Conversion, University of Delaware) for providing access and assistance to the XRD unit. Thanks to Ken Levi (Johns Hopkins University) for providing access to the electron microprobe. Jeffery Post (Smithsonian Institute) provided Zn mineral references. This manuscript benefited from the reviews of three anonymous reviewers. D.R. Roberts appreciates the support of a National Science Foundation graduate research fellowship.

Literature Cited

- (1) Dudka, S.; Adriano, D. C. *J. Environ. Qual.* **1997**, *26*, 590–602.
- (2) McBride, M. B. *Environmental Chemistry of Soils*; Oxford University Press: New York, 1994.
- (3) Chaney, R. L. In *Zinc in Soils and Plants*; Robson, A. D., Ed.; Kluwer Academic Publishers: The Netherlands, 1993; pp 135–144.
- (4) Adriano, D. C. *Trace Elements in the Terrestrial Environment*; Springer-Verlag: New York, 1986.
- (5) Zasoski, R. J.; Burau, R. G. *Soil Sci. Soc. Am. J.* **1988**, *52*, 81–87.
- (6) Stahl, R. S.; James, B. R. *Soil Sci. Soc. Am. J.* **1991**, *55*, 1291–1294.
- (7) Murray, J. W. *Geochim. Cosmochim. Acta* **1975**, *39*, 505–519.
- (8) Melis, P.; Manunsa, B.; Premoli, A.; Gessa, C. Z. *Pflanzenernähr. Bodenk.* **1987**, *150*, 99–102.
- (9) Kinniburgh, D. G.; Jackson, M. L.; Syers, J. K. *Soil Sci. Soc. Am. J.* **1976**, *40*, 796–799.
- (10) Huang, C. P.; Rhoads, A. J. *Colloid Interface Sci.* **1989**, *131*, 289–306.
- (11) Spark, K. M.; Wells, J. D.; Johnson, B. B. *Eur. J. Soil Sci.* **1995**, *46*, 633–640.
- (12) Ladonin, D. V. *Eurasian Soil Sci.* **1997**, *30*, 1478–1485.
- (13) Sadiq, M. *Water, Air, Soil Pollut.* **1991**, *57–58*, 411–421.
- (14) Metwally, A. I.; Mashhady, A. S.; Falatah, A. M.; Reda, M. Z. *Pflanzenernähr. Bodenk.* **1993**, *156*, 131–135.
- (15) Gerth, J.; Brümmer, G. W.; Tiller, K. G. Z. *Pflanzenernähr. Bodenk.* **1992**, *156*, 123–129.
- (16) Brümmer, G. W.; Gerth, J.; Tiller, K. G. *J. Soil Sci.* **1988**, *39*, 37–52.
- (17) Manceau, A.; Schlegel, M. L.; Musso, M.; Sole, V. A.; Gauthier, C.; Petit, P. E.; Trolard, F. *Geochim. Cosmochim. Acta* **2000**, *64*, 3643–3661.

- (18) Ford, R. G.; Sparks, D. L. *Environ. Sci. Technol.* **2000**, *34*, 2479–2483.
- (19) Trainor, T. P.; Brown, G. E., Jr.; Parks, G. A. *J. Colloid Interface Sci.* **2000**, *231*, 359–372.
- (20) Schlegel, M. L.; Manceau, A.; Charlet, L. *J. Phys. IV* **1997**, *7*, 823–824.
- (21) Bochatay, L.; Persson, P. *J. Colloid Interface Sci.* **2000**, *229*, 593–599.
- (22) Hesterberg, D.; Sayers, D. E.; Zhou, W.; Plummer, G. M.; Robarge, W. *Environ. Sci. Technol.* **1997**, *31*, 1.
- (23) O'Day, P. A.; Carroll, S. A.; Waychunas, G. A. *Environ. Sci. Technol.* **1998**, *32*, 943–955.
- (24) Webb, S. M.; Leppard, G. G.; Gaillard, J.-F. *Environ. Sci. Technol.* **2000**, *34*, 1926–1933.
- (25) Manceau, A.; Lanson, B.; Schlegel, M. L.; Hargé, J. C.; Musso, M.; Eybert-Bérard, L.; Hazemann, J.-L.; Chateigner, D.; Lamble, G. M. *Am. J. Sci.* **2000**, *300*, 289–343.
- (26) de Groot, A. J. In *Metal Contaminated Aquatic Sediments*; Allen, H. E., Ed.; Ann Arbor: Chelsea, 1995; pp 1–80.
- (27) Manceau, A.; Boisset, M. C.; Sabet, G.; Hazemann, J.; Mench, M.; Cambier, P.; Prost, R. *Environ. Sci. Technol.* **1996**, *30*, 1540–1552.
- (28) Morin, G.; Ostergren, J. D.; Juillot, F.; Ildefonse, P.; Calas, G.; Brown, G. E., Jr. *Am. Mineral.* **1999**, *84*, 420–434.
- (29) Morris, D. E.; Allen, P. G.; Berg, J. M.; Chisholm-Brause, C. J.; Conradson, S. D.; Donohoe, R. J.; Hess, N. J.; Musgrave, J. A.; Tait, C. D. *Environ. Sci. Technol.* **1996**, *30*, 2322–2331.
- (30) Ostergren, J. D.; Brown, G. E., Jr.; Parks, G. A.; Tingle, T. N. *Environ. Sci. Technol.* **1999**, *33*, 1627–1636.
- (31) Hunter, D. B.; Bertsch, P. M. *J. Radioanal. Nucl. Chem.* **1998**, *234*, 237–242.
- (32) Bertsch, P. M.; Hunter, D. B. In *Future of Soil Chemistry*; Huang, P. M., Sparks, D. L., Boyd, S. A., Eds.; Soil Sci. Soc. Am.: Madison, WI, 1998; Vol. SSSA Spec. Publ. 55, pp 103–122.
- (33) Storm, G. L.; Yahner, R. H.; Bellis, E. D. *Arch. Environ. Contam. Toxicol.* **1993**, *25*, 428–437.
- (34) Buchauer, M. *J. Environ. Sci. Technol.* **1973**, *7*, 131–135.
- (35) Lalo, J. *Am. Forests* **1988**, *March/April*, 55–69.
- (36) Schwertmann, U.; Cornell, R. M. *Iron Oxides in the Laboratory: Preparation and Characterization*; Weinheim: New York City, 1991.
- (37) McKenzie, R. M. *Miner. Magn.* **1971**, *38*, 493–502.
- (38) Lin, Z.; Herbert, R. B., Jr. *Environ. Geol.* **1997**, *33*, 1–12.
- (39) Rose, S.; Ghazi, A. *Environ. Geol.* **1998**, *36*, 364–370.
- (40) Lytle, F. W.; Gregor, R. B.; Sandstorm, D. R.; Marques, E. C.; Wong, J.; Spiro, C. L.; Huffman, G. P.; Huggins, F. E. *Nucl. Instrum. Methods Phys. Res.* **1984**, 542–548.
- (41) MacDowell, A. A.; Celestre, R.; Chang, C. H.; Lamble, G. M.; Padmore, H. A.; Patel, J. R. In *X-ray microfocusing: Applications and Techniques*; McNulty, L., Ed., 1998; pp 137–144.
- (42) Zabinsky, S. L.; Rehr, J. J.; Ankudinov, A.; Albers, R. C.; Eller, M. *J. Phys. Rev. B: Condens. Matter* **1995**, *52*, 2995–3006.
- (43) Scheidegger, A. M.; Lamble, G. M.; Sparks, D. L. *J. Colloid Interface Sci.* **1997**, *186*, 118–128.
- (44) Ressler, T. *J. Synchrotron Rad.* **1998**, *5*, 118–122.
- (45) Strawn, D. G.; Sparks, D. L. *Soil Sci. Soc. Am. J.* **1998**, *64*, 144–156.
- (46) Doriguetto, A.; Fernandes, N. *Acta Crystallogr., Sect. C* **1999**, *55*, 1751–1753.
- (47) Barak, P.; Helmke, P. A. In *Zinc in Plants and Soils*; Robson, A. D., Ed.; Kluwer Academic: Dordrecht, The Netherlands, 1993; pp 1–13.
- (48) Lindsay, W. L. *Chemical Equilibria in Soils*; John Wiley and Sons: New York, 1979.
- (49) Elgersma, F.; Schinkel, J. N.; Weijnen, M. P. C. In *Heavy Metals: Problems and Solutions*; Salomons, W., Förstner, U., Mader, P., Eds.; Springer-Verlag: Berlin, 1995; pp 193–235.
- (50) Venditti, D.; Berthelin, J.; Durécu, S. *Arch. Environ. Contam. Toxicol.* **2000**, *38*, 421–427.

Received for review May 7, 2001. Revised manuscript received December 14, 2001. Accepted December 19, 2001.

ES015516C